Postprint

A Simplified Interference Model for Outdoor Millimeter-wave Networks

Xiaolin Jiang[1] · **Hossein Shokri-Ghadikolaei**[1] ·
Carlo Fischione[1] · **Zhibo Pang**[2]

Abstract Industry 4.0 is the emerging trend of the industrial automation. Millimeter-wave (mmWave) communication is a prominent technology for wireless networks to support the Industry 4.0 requirements. The availability of tractable accurate interference models would greatly facilitate performance analysis and protocol development for these networks. In this paper, we investigate the accuracy of an interference model that assumes impenetrable obstacles and neglects the sidelobes. We quantify the error of such a model in terms of statistical distribution of the signal to noise plus interference ratio and of the user rate for outdoor mmWave networks under different carrier frequencies and antenna array settings. The results show that assuming impenetrable obstacle comes at almost no accuracy penalty, and the accuracy of neglecting antenna sidelobes can be guaranteed with sufficiently large number of antenna elements. The comprehensive discussions of this paper provide useful insights for the performance analysis and protocol design of outdoor mmWave networks.

1 Introduction

Industry 4.0, or the fourth industrial revolution is the current trend of the industrial automation [1]. It is based on Internet of Things, which enables the industrial

Xiaolin Jiang
E-mail: xiaolinj@kth.se

Hossein Shokri-Ghadikolaei
E-mail: hshokri@kth.se

Carlo Fischione
E-mail: carlofi@kth.se

Zhibo Pang
E-mail: pang.zhibo@se.abb.com

[1] KTH Royal Institute of Technology,Stockholm, Sweden ·
[2] ABB Corporate Research, Västerås, Sweden

modules to communicate and cooperate with each other in real time. In addition to many indoor industrial applications, there are many outdoor industrial applications that can be covered by our work. Examples include open pit mining, where controlled blasting are used to enhance productivity and ensure the safety of the workers [2]. Also, the power systems automation has outdoor applications, including distribution automation (namely, the automatic control of the various smart grids units that are distributed over the grid) and integration of distributed renewable energy sources and storages [3]. The industrial manufacturing requires high reliability and stringent delay guarantee, which is usually realized by wired communication links. However, to support mobility, flexibility, and to eliminate the heavy and expensive cables, wireless communication is the promising solution for the future industrial networks [4]. References [5] and [6] investigate the requirements of the wireless communication to support critical control applications.

Millimeter-wave (mmWave) communications are a promising candidate to realize wireless network of Industry 4.0, as it has abundant bandwidth to support high data rate, which is essential for the high-data rate applications like the real-time video delivery [7,8]. Moreover, the delay spread of mmWave is lower than that of the microwave band, which helps reduce the guard interval for the inter-symbol interference mitigation and consequently improve the transmission efficiency [9]. This is particularly important for the mission critical industrial applications due to their tight latency and reliability requirements.

The availability of accurate interference models is essential to evaluate the performance of mmWave networks, to design proper protocols for different communication layers, and to optimize the network performance. However, exact or very accurate interference models are generally quite complex and sometimes mathematically intractable. Interference models with different accuracy and complexity have been used in the literature. A simple interference model considering infinite penetration loss and no sidelobe transmission/reception is used to develop multihop medium access control (MAC) layer in mmWave wireless networks [10]. [11] assumes no emissions from the antenna sidelobe, while [12] considers impenetrable obstacle and negligible sidelobe gain as the interference model in a random mmWave ad hoc network. This simple interference model enables deriving tractable closed-form expressions for the main performance metrics and delivering useful design insights. However, the accuracy of the underlying interference model is not therein quantified, thus whether the simplified interference methods achieve good balances between the simplicity and accuracy is not known.

In [13,14], the blockage is modeled by a line-of-sight (LOS) ball, i.e., all the transmitters within a certain distance of the receiver (located at the center of the ball) are always in the LOS condition, and all the transmitters outside this ball have a non-LOS condition. This approximation greatly simplifies mathematical analysis. This blockage model is extended to two-ball model [15], where transmitters outside the outer ball will be always in an outage condition, namely they will not cause any interference to the receiver located at the origin of the balls. [16] proposes smart scheduling with relays to overcome the blockage in the mmWave communications, which shortens the link distance and lower the interference. The accuracy of such interference model comes at the price of complexity and less tractability. In [17], an index is proposed that allows quantifying the accuracy of any interference model. The authors also show that as the directionality increases
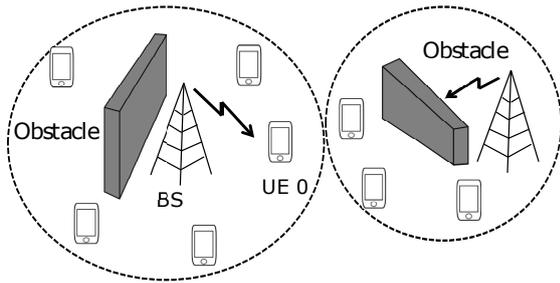
Fig. 1 Outdoor mmWave network. The dashed lines show the base station coverage boundaries, and may not be that regular in practice.

(e.g., by beamforming with more antennas), simpler interference models may be sufficiently accurate.

In this paper, we propose a complementary method to assess the accuracy of a simplified interference model, namely assuming impenetrable obstacles and no antenna sidelobes. We investigate the accuracy index defined in [17] and the relative difference in 50th percentile rate under a uniform planar array (UPA) of antennas at 28 GHz and at 73 GHz with different base station (BS) density and obstacle density. The results show that the assumption of impenetrable obstacles introduces negligible loss in the accuracy of the interference model, thanks to the special characteristics of the mmWave communications. Moreover, considering no sidelobes may cause non-negligible accuracy loss with small antenna size, which can be compensated by increasing the number of antenna elements.

The rest of this paper is organized as follows. Section 2 presents our system model. In Section 3, we represent the interference model similarity index and introduce our performance metrics. In Section 4, we investigate the accuracy of the interference model assuming infinite penetration loss or/and negligible antenna sidelobes. Concluding remarks are provided in Section 5.

2 System model

We consider a downlink scenario for an outdoor network operating at the mmWave frequencies. The number of BSs and obstacles are random variables with densities λ_b and λ_o per square kilometer respectively, and they are randomly uniformly distributed in the plane, as shown in Fig. 1. We assume that each obstacle has a rectangular shape with a random width that is independently uniformly taken from [0,5] meters, a random length uniformly taken from [0,10] meters, and a random orientation that is independently uniformly taken from [0,2π]. Almost all obstacles can be approximated with one of those random rectangles in the outdoor environment. With the BS density being λ_b/km^2, the size of a typical cell is $1/\lambda_b$ km^2.

We study the performance of a reference user equipment UE 0 located at the origin of the Cartesian coordinate, which will be associated to the BS with the smallest pathloss. We consider a single path narrowband geometrical channel model between every BS to its serving UE [8]. Then, the downlink channel response

Table 1 Channel Model Parameters, Based on [7], [8].

	c	α	n
28 GHz	61.4 dB	1.15×10^{-5}	5.8 dB
73 GHz	69.8 dB	2.76×10^{-5}	5.8 dB

between BS i and UE j is given by

$$\mathbf{H}_{ij} = \sqrt{N_t N_r}\, g_{ij}\, \mathbf{a}_{\mathrm{UE}}\left(\phi_{ij}^{\mathrm{UE}}, \theta_{ij}^{\mathrm{UE}}\right)\left(\mathbf{a}_{\mathrm{BS}}\left(\phi_{ij}^{\mathrm{BS}}, \theta_{ij}^{\mathrm{BS}}\right)\right)^*, \tag{1}$$

where N_t and N_r are the number of antenna elements at the transmitter side and at the receiver side, ϕ_{ij}^{UE} and $\theta_{ij}^{\mathrm{UE}}$ are the horizontal and vertical angles of arrival (AoA) at the UE j from BS i, ϕ_{ij}^{BS} and $\theta_{ij}^{\mathrm{BS}}$ are the horizonal and vertical angles of departure (AoD) from the BS i to UE j, $\mathbf{a}_{\mathrm{BS}}\left(\phi_{ij}^{\mathrm{BS}}, \theta_{ij}^{\mathrm{BS}}\right)$ and $\mathbf{a}_{\mathrm{UE}}\left(\phi_{ij}^{\mathrm{UE}}, \theta_{ij}^{\mathrm{UE}}\right)$ are normalized array responses to the AoD and AoA along this link, and $(\cdot)^*$ is the Hermitian operator. We consider half-wavelength UPAs of size $N_b \times N_b$ at the BSs and of size $N_u \times N_u$ at the UEs. For half wavelength UPA of $N \times N$ antennas, we have [18]

$$\mathbf{a}\left(\phi, \theta\right) = \frac{1}{N}[1, \ldots, e^{j\pi(m\sin\phi\sin\theta + n\cos\theta)}, \ldots, e^{j\pi((N-1)\sin\phi\sin\theta + (N-1)\cos\theta)}]^*, \tag{2}$$

where $0 \le m < N$, and $0 \le n < N$ are the indices of an antenna element along the two dimensions in the UPA array. The antenna pattern can be easily extended to others by replacing $\mathbf{a}_{\mathrm{BS}}$ and $\mathbf{a}_{\mathrm{UE}}$ according to the new patterns. The term g_{ij} in (1) is a zero-mean complex Gaussian random variable with variance $10^{-0.1 L_{ij}}$, where L_{ij} is the path loss in dB [8]. The path loss consists of a constant attenuation, a distance dependent attenuation, penetration losses caused by the obstacles, and a large scale lognormal fading. Let d_{ij} be the distance between BS i and UE j (path length) in meters, n_{ij} be the number of obstacles in this path, l_o be the penetration loss of each obstacle in dB, α be the attenuation factor due to atmospheric absorbtion, and $l_\alpha = 10\log(e^{\alpha d_{ij}})$ be the absorption loss in dB. Then, the path loss is

$$L_{ij}\,[\mathrm{dB}] = c + 20\log(d_{ij}) + l_\alpha + n_{ij}l_o + X\,, \tag{3}$$

where c is a constant attenuation, and X represents the shadowing component of the path-loss, and is a zero-mean i.i.d. Gaussian random variable with standard deviation n. Parameters of channel model (3) depend on the carrier frequency and are provided in Table 1.

We assume a universal frequency reuse, so all non-serving BSs can cause interference to the reference receiver, UE 0. The associated BS is indexed by 0, and the set of all interfering BSs is denoted by $\mathcal{I}$. Then, the SINR at UE 0 is

$$\gamma = \frac{p_0\left|\left(\mathbf{w}_0^{\mathrm{UE}}\right)^{\mathrm{H}}\mathbf{H}_{00}\,\mathbf{w}_0^{\mathrm{BS}}\right|^2}{\sum\limits_{i \in \mathcal{I}} p_i\left|\left(\mathbf{w}_0^{\mathrm{UE}}\right)^{\mathrm{H}}\mathbf{H}_{i0}\,\mathbf{w}_i^{\mathrm{BS}}\right|^2 + \sigma}\,, \tag{4}$$

where p_i is the transmission power of BS i, σ is the noise power, $\mathbf{w}_0^{\mathrm{UE}}$ is the combining vector at UE 0, and $\mathbf{w}_i^{\mathrm{BS}}$ denotes the precoding vector at BS i. To

reduce the complexity and cost of beamforming, we assume an analog precoder both at the BSs and at the UEs; however, the framework of this paper can be easily extended to other beamforming strategies. At each BS, the transmitting beam is matched to the AoD direction to its associated UE. Similarly, the combining vector at each UE i is matched to the AOA from its serving BS. That is given BS i will serve UE j, $\mathbf{w}_i^{\mathrm{BS}} = \mathbf{a}_{\mathrm{BS}}\left(\phi_{ij}^{\mathrm{BS}}, \theta_{ij}^{\mathrm{BS}}\right)$ and $\mathbf{w}_j^{\mathrm{UE}} = \mathbf{a}_{\mathrm{UE}}\left(\phi_{ij}^{\mathrm{UE}}, \theta_{ij}^{\mathrm{UE}}\right)$. This precoding and combining vectors can maximize the link SNR, namely $|(\mathbf{w}_j^{\mathrm{UE}})^* \mathbf{H}_{ij} \mathbf{w}_i^{\mathrm{BS}}|^2$, see [19].

An interference model attempts at modeling different components of (3). For mathematical tractability, usually, antenna pattern or channel models are simplified. These approximations make it possible to evaluate the SINR distribution and thereby performance metrics such as the data rate. However, the derived SINR distribution may not necessarily be close to the actual SINR[1] distribution before all those approximations. In the next section, we introduce two metrics that allow quantifying the closeness of two statistical distributions.

3 Measuring Accuracy of SINR and Rate Analysis

Consider a reference interference model y, which results in SINR γ^{y} with distribution $f_{\gamma^{\mathrm{y}}}(t)$, and any test interference model x, which results in SINR γ^{x} with distribution $f_{\gamma^{\mathrm{x}}}(t)$. In the following, we consider the interference model accuracy index [17] and the relative difference in the 50th percentile rate. These two metrics allow analyzing closeness of two probability distribution functions (PDFs), and thereby assessing the accuracy of SINR and rate analysis when using a simple interference model in mmWave networks.

3.1 Interference Model Accuracy Index

The interference model accuracy (IMA) index describes how close the PDF of γ^{x} is compared to PDF of γ^{y}. To formally define IMA index, let $\beta > 0$ denote the SINR threshold corresponding to a certain target bit error rate, then an outage on the receiver occurs when $\gamma < \beta$. Suppose that the interference model y can perfectly capture outage events. Let hypotheses H_0 and H_1 denote the absence (i.e., $\gamma^{\mathrm{y}} \geq \beta$) and the presence (i.e, $\gamma^{\mathrm{y}} < \beta$) of outage under reference model y. A false alarm for interference model γ^{x} corresponds to the event that x declares outage under hypothesis H_0 (i.e., no harmful interference is present); whereas a miss-detection corresponds to the event that x fails to identify outage under hypothesis H_1. For any constant $0 \leq \xi \leq 1$, the interference model accuracy index is defined as

$$\mathrm{IMA}\left(\mathrm{x}, \mathrm{y}, \xi, \beta\right) = \xi \left(1 - p_{\mathrm{fa}}^{\mathrm{x|y}}(\beta)\right) + (1 - \xi) \left(1 - p_{\mathrm{md}}^{\mathrm{x|y}}(\beta)\right), \tag{5}$$

where $p_{\mathrm{fa}}^{\mathrm{x|y}}(\beta) = \Pr\left[\gamma^{\mathrm{x}} < \beta \mid \gamma^{\mathrm{y}} \geq \beta\right]$ is the false alarm probability, and $p_{\mathrm{md}}^{\mathrm{x|y}}(\beta) = \Pr\left[\gamma^{\mathrm{x}} \geq \beta \mid \gamma^{\mathrm{y}} < \beta\right]$ is the miss-detection probability. $\mathrm{IMA}\left(\mathrm{x}, \mathrm{y}, \xi, \beta\right)$ is a unit-less

---

[1] actual SINR corresponds to the SINR when l_o is the exact penetration loss of each obstacle in (3) and the sidelobe gain is considered.

real-valued quantity ranging within $[0, 1]$, where higher values represent higher similarity between x and y. By setting $\xi = \Pr\left[\gamma^y \geq \beta\right]$, parameter $\mathrm{IMA}\left(\mathrm{x}, \mathrm{y}, \Pr\left[\gamma^y \geq \beta\right], \beta\right)$ is equal to the average probability that interference model x gives the same decision as the reference model y.

We define the minimum IMA index as,

$$\min \mathrm{IMA}\left(\mathrm{x}, \mathrm{y}\right) = \min_{\beta} \mathrm{IMA}\left(\mathrm{x}, \mathrm{y}, \Pr\left[\gamma^y \geq \beta\right], \beta\right). \tag{6}$$

The term $\min \mathrm{IMA}\left(\mathrm{x}, \mathrm{y}\right)$ shows the minimum value (worst case) of the accuracy of interference model x compared to the reference model y.

3.2 The Relative Difference in the 50th Percentile Rate

The transmit data rate is an important index to assess the network performance. We consider maximum achievable rate as

$$\mathrm{Rate} = \mathrm{B}\log_2(1+\gamma), \tag{7}$$

where B is the bandwidth and γ is the SINR. The rate coverage as the complementary cumulative distribution function of rate is

$$P(\rho) = \Pr(\mathrm{Rate} > \rho), \tag{8}$$

where ρ is the rate threshold that determines different rate coverage values. With a large amount of Monte Carlo simulation, we obtain a set of rate values that the reference receiver observes. We then determine the distribution and also 50% of rate from this set. Denote the 50th percentile rate calculated by interference model x and y by $\rho^x_{50\mathrm{th}}$ and $\rho^y_{50\mathrm{th}}$ respectively, which satisfy $\Pr(\mathrm{Rate}_x > \rho^x_{50\mathrm{th}}) = 50\%$ and $\Pr(\mathrm{Rate}_y > \rho^y_{50\mathrm{th}}) = 50\%$. Besides rate coverage, we calculate the relative difference in the 50th percentile rates calculated by two interference models x and y as a metric of accuracy of rate analysis:

$$\mathrm{Rate}_{\mathrm{diff}-50\%} = \frac{|\rho^x_{50\mathrm{th}} - \rho^y_{50\mathrm{th}}|}{\rho^y_{50\mathrm{th}}}. \tag{9}$$

Similarly with $\min \mathrm{IMA}$, $\mathrm{Rate}_{\mathrm{diff}-50\%}$ can also capture the biggest gap between two rate distribution and can very well characterize the similarity between using simplified interference model or not. The parameter $\min \mathrm{IMA}$ ranges within $[0, 1]$ with higher value representing better similarity, while $\mathrm{Rate}_{\mathrm{diff}-50\%}$ ranges within $[0, \infty]$ with smaller value representing better similarity.

4 Simplified Interference Model for Outdoor MmWave Networks

Interference models in mmWave networks are generally very complicated due to both blockage and directionality. An accurate interference model should include a complex channel model whose parameters are very different in LOS and non-LOS conditions. This LOS condition, per se, is a random event whose probability depends on the distance between transmitter and receiver. Accurate interference models should also include antenna gains (both at the transmitter and at the
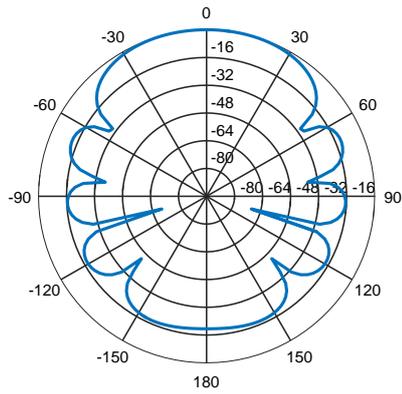
(a) Actual antenna gain.
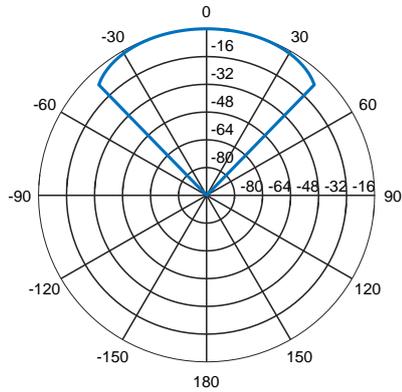
(b) Simplified antenna gain.

Fig. 2 Actual and simplified antenna gains. All the gains are in dB.

receiver), which depend on the network topology and antenna patterns. Simplifying the blockage model and antenna patterns, as done in [10], will significantly increase tractability of mathematical performance evaluation and optimization of mmWave networks, and can lead to better design insights. These insights are valid as long as the underlying simple interference model is of sufficient accuracy. In the following, we investigate the accuracy of such interference model.

We consider a "realistic" reference physical model y with a finite penetration loss and actual antenna pattern, created by the analog precoding and combining vectors. We then approximate such simplified interference model by x wherein we consider infinite penetration loss and no antenna sidelobes. Fig. 2 shows the actual and simplified antenna gain on the horizontal plane as a function of angular distance from the antenna boresight for the 8×8 UPAs. Fig. 2(a) corresponds to the actual antenna pattern of UPA in the horizontal domain, and Fig. 2(b) corresponds to the simplified antenna pattern (zero outside the main lobe). With more antenna elements, the beamwidth of the main lobe and sidelobe decreases. Moreover, the strongest sidelobe gain also decreases with the number of antenna elements.
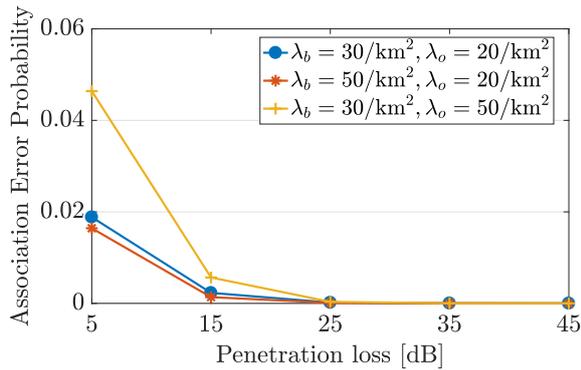
Fig. 3 Association error probability when considering impenetrable obstacles.

To evaluate the effect of infinite penetration loss assumption, we consider a test model x_a with $l_o = \infty$ in (3). Other parameters of x_a are similar to those of y. To evaluate the effect of the no-sidelobe approximation, we take a test model x_b similar to y except that the sidelobe gain is ignored in x_b. Finally, we investigate the joint effect of the two assumptions by considering a test model x_c with infinite penetration loss and no sidelobe. The 28GHz band is 27.5-29.5GHz, and the 73GHz band is from 71GHz to 76GHz. In the following and without loss of generality, we consider 30 dBm transmission power, 500 MHz bandwidth (so -87 dBm noise power).

4.1 Impact of Assuming Infinite Penetration Loss

In this subsection, we study the error due to the impenetrable obstacles assumption. As the rule is to associate UE 0 to the BS with the smallest pathloss before beamforming, and when considering infinite penetration loss, UE 0 can only be associated to a LOS BS. An association error occurs only when there is a non-LOS BS that has a smaller pathloss. Considering 8×8 UPA antennas at the BSs and 4×4 UPA antennas at the UEs, Fig. 3 presents the association error probability, and this association error probability decreases with the increase of penetration loss for each obstacle. With 5 dB penetration loss and $\lambda_o = 50/\text{km}^2$, the error probability is around 5%. However, we should note that typical penetration loss values in mmWave is higher than 15 dB, for which the association error probability can be neglected, i.e., assuming impenetrable obstacles will not sensibly affect the association decisions, given association based on the smallest path-loss.

Next, we evaluate the impact of assuming impenetrable obstacles on the SINR distribution. First, we note that with infinite penetration loss, only the LOS BSs can cause interference to UE 0, whereas every BS causes interference to UE 0 when the penetration loss is finite. Fig. 4 shows $\min \text{IMA}$ against the penetration loss in y (it is always ∞ in x_a). To calculate $\min \text{IMA}$, we sweep β from 0 to 30dB to capture the smallest accuracy value in this SINR threshold region. From this figure, assuming impenetrable obstacles is more accurate for higher penetration loss values. Moreover, the accuracy index increases with the density of BSs, as more BSs is equivalent to shorter distances between the interfering BSs and UE
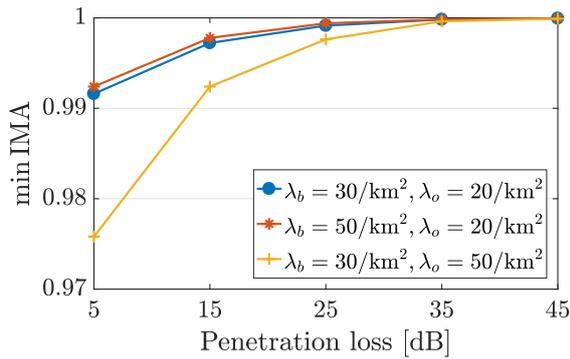
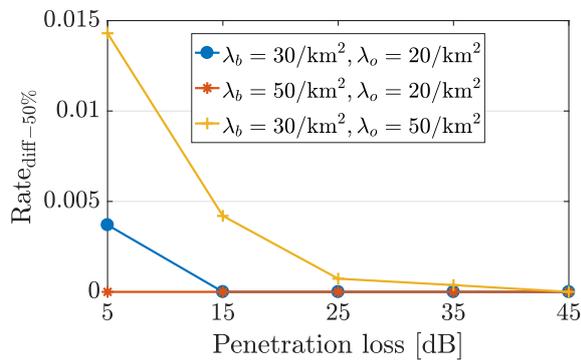**Fig. 4** Impact of infinite penetration loss on $\min \mathrm{IMA}$.

Fig. 5 Impact of infinite penetration loss on $\mathrm{Rate}_{\mathrm{diff}-50\%}$.

0, and higher likelihood of having interferes with LOS condition to the UE 0. The contribution of these LOS interferes in the aggregated interference term dominates that of non-LOS interferes. For penetration loss less than 15 dB, the assumption of impenetrable obstacle reduces $\min \mathrm{IMA}$ by less than 1% when the obstacle density is $20/\mathrm{km}^2$. On the other hand, the accuracy index expectedly decreases with the density of obstacles, The accuracy loss, however, is very limited, e.g., only 1% additional loss when increasing the obstacle density from $20/\mathrm{km}^2$ to $50/\mathrm{km}^2$ for the penetration loss of 5 dB. Even this such small loss vanishes when the penetration loss is larger than 35 dB.

Fig. 5 shows $\mathrm{Rate}_{\mathrm{diff}-50\%}$ between y and x_a. For all the three curves, when the penetration loss in y equals 5 dB, the assumption of impenetrable obstacle causes less than 1.5% difference for the rate coverage, and this difference ratio further decreases to less than 0.2% with each obstacle penetration loss larger than 15 dB in y. Similarly as Fig. 4, $\mathrm{Rate}_{\mathrm{diff}-50\%}$ decreases with the density of BSs, and minimal difference exists when $\lambda_b = 50/\mathrm{km}^2$ and penetration loss larger than 15 dB.

Overall, the assumption of impenetrable obstacles introduces negligible loss in calculating SINR and rate distributions, but improves the mathematical tractabil-
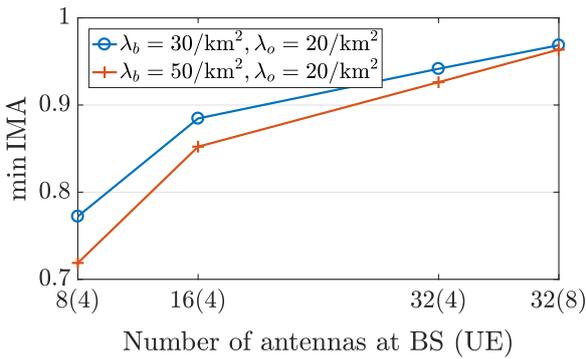
Fig. 6 Impact of ignoring antenna sidelobes on min IMA. Antenna elements are in the form of UPA of N×N antennas.

ity. This assumption works very well in mmWave networks with denser BS deployments.

4.2 Impact of Neglecting Antenna Sidelobes

Under the no-sidelobe assumption, in (4), if the main beam of the interference caused by BS i does not lie in the main beam of UE 0, the term $\left|\left(\mathbf{w}_0^{\mathrm{UE}}\right)^{\mathrm{H}} \mathbf{H}_{i0} \mathbf{w}_i^{\mathrm{BS}}\right|^2$ corresponding to the interference component from BS i will be set to zero. Fig. 6 presents the effect of neglecting the sidelobes. The antenna pattern at BSs and UEs are set as the parameters at the x label. Neglecting the sidelobes can lead to clear difference between x_b and y, and more than 20% accuracy loss occurs with 8×8 UPAs at BSs, and 4×4 UPAs at the UEs. The accuracy index increases with the number of of antennas at each side, as more antennas enable narrower beamwidth and less sidelobe gain, e.g., the min IMA indexes increase from 0.73 to 0.96, and from 0.86 to 0.97 respectively with the antenna number increase from 8×8 UPA to 32×32 UPA at BSs, and 4×4 UPA to 8×8 UPA at UEs in the two scenarios. It is also observed that the min IMA index decreases with more interfering BSs, as the increased aggregated interferers lead to less similarity between the two models.

Ignoring antenna sidelobes can also introduce a noticeable difference to the rate distribution, as shown in Fig. 7. With dense BS deployment and moderate number of antennas at both BS and UE, Rate$_{\mathrm{diff}-50\%}$ is as large as 39%. With the increase of the number of the antenna elements, Rate$_{\mathrm{diff}-50\%}$ of the two scenarios decreases to around 5% when using 16×16 UPA at the BS side. The loss in the calculation of the rate further vanishes by increasing the number of antenna elements at the transmitter/receiver.

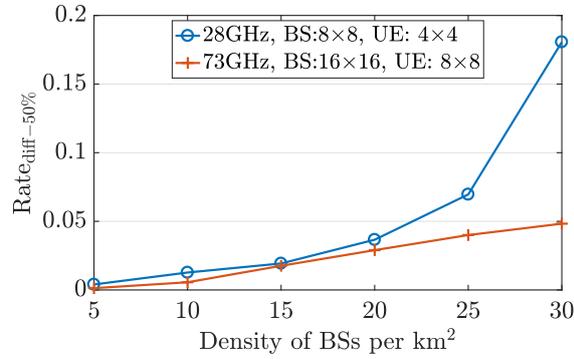### 4.3 Joint Impact of Assuming Infinite Penetration Loss and Neglecting Antenna Sidelobes

In this subsection, we consider the joint impact of assuming infinite penetration loss together with zero sidelobe. In y, the penetration loss of each obstacle is 15
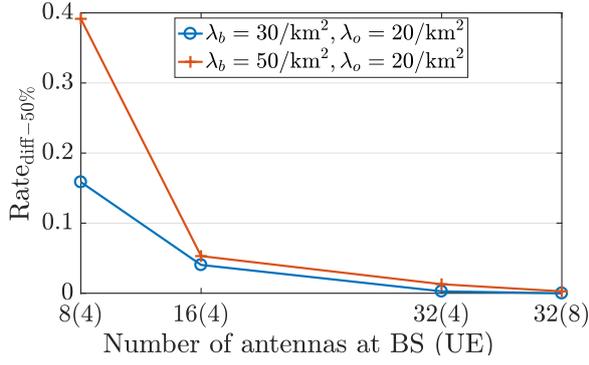
Fig. 7 Impact of ignoring antenna sidelobes on $\mathrm{Rate}_{\mathrm{diff}-50\%}$. Antenna elements are in the form of UPA of N×N antennas.
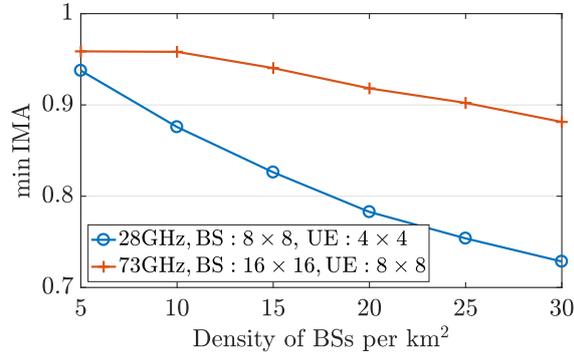
Fig. 8 Impact of assumption of impenetrable obstacle and no sidelobe on $\min \mathrm{IMA}$ with λ_o=20/km^2.

Fig. 9 Impact of assumption of impenetrable obstacle and no sidelobe on $\mathrm{Rate}_{\mathrm{diff}-50\%}$ with λ_o=20/km^2.

dB and with sidelobes, while in x$_c$, the obstacles are with infinite penetration loss and no sidelobe. The min IMA at 28 GHz and 73 GHz are simulated with different

density of BSs. The antenna size at the two frequencies are kept nearly the same. At 28 GHz, we consider 8×8 UPAs at the BSs and 4×4 UPAs at the UEs; while at 73 GHz, we consider 16×16 UPAs at the BSs and 8×8 UPAs at the UEs. When increasing frequency, the wavelength as well as the distance between antennas decreases, enabling more antennas to be mounted at the same size. In Fig. 8, the accuracy decreases with the density of BSs, which is in accordance to neglecting sidelobe. The difference between the min IMA indexes of the two frequencies is only around 2% with the BS density equals $5/\text{km}^2$, however, this difference grows to 15% when $\lambda_b = 30/\text{km}^2$. With more antennas at higher frequencies, the mainlobe and sidelobe are narrower, the accuracy can be improved. The min IMA index decreases more slowly at higher frequency with more antenna elements. When the BS density increases from $5/\text{km}^2$ to $30/\text{km}^2$, the accuracy loss of the 73 GHz just has a 8% decrease compared to a nearly 20% at 28 GHz.

Fig. 9 illustrates the difference of the rate distribution between x_c and y. Expectedly, the $\text{Rate}_{\text{diff}-50\%}$ of 73 GHz is smaller than that of 28 GHz at all BS densities. Though the different parameters of the channel model in the two frequencies also have some minor effect to the different performance, the difference is mainly caused by the different number of antenna at the two sides. The more focused beams at the 73 GHz further improve the link budget while reducing the interference term. Therefore, the rate that UE 0 experiences under simplified reference model is closer to the actual rate at 73 GHz compared to that of 28 GHz. That is, the simplified interference model becomes more accurate at 73 GHz. The $\text{Rate}_{\text{diff}-50\%}$ of 73 GHz is smaller than 5% for all the BS densities in the figure, while the $\text{Rate}_{\text{diff}-50\%}$ of 28 GHz shoots to 18% when $\lambda_b = 30/\text{km}^2$.

Overall, it causes non-neglegible loss to the accuracy of the interference model and rate distribution similarity by ignoring sidelobes alone and the joint effect by considering impenetrable obstacles and no sidelobe. However this loss can be kept to a smaller value when manufacturing large number of antenna elements at both the BS and UE side. Besides increasing the antenna elements, in reality, different frequencies may be used between adjacent BSs to mitigate the interference, so the number of interfering BSs should be much less than the total number of BSs. Proper scheduling to regulate the BSs transmitting simultaneously can also help to increase the min IMA index and lower $\text{Rate}_{\text{diff}-50\%}$ significantly.

5 Conclusions

We proposed a simplified interference model in outdoor mmWave networks that considers infinite penetration loss and no sidelobe, and investigated the similarity of SINR and rate distributions between this simplified model with realistic model with an interference model accuracy index and the relative difference in the 50th percentile rate. The impact of the first assumption on the accuracy of the simplified interference model can be neglected, while the impact of considering no sidelobe can not be neglected in denser BS settings. However, by increasing the number of antennas can increase the accuracy. In particular, with 16×16 UPAs at the BSs, 8×8 at the UEs, the accuracy loss of the interference model and the according relative difference in the 50th percentile rate are less than 5% when the density of BSs does not exceed $30/\text{km}^2$. The accuracy index can be further improved by effective frequency reuse and proper scheduling to limit the number of interfer-

ing BSs transmitting simultaneously. MmWave network itself is very complicated due to the difficulty to characterize the propagation under different environment. Combination between mmWave and mission critical industrial applications make it even more challenging as mission critical industrial applications further add more difficulties at the higher layers. The simplified interference model can be a good base for the research of mmWave networks combined with mission critical industrial applications to support the Industry 4.0 scenarios. As the transmission frequency is lower than the cellular network, the presence of less simultaneous transmission can lead to even higher accuracy for the simplified model.

References

1. Schwab, K.: The fourth industrial revolution. Geneva: World Economic Forum, 2016.
2. Mishra,A. K., Nigam, Y., Singh, D. R.: Controlled blasting in a limestone mine using electronic detonators: A case study. J. Geol. Soc. India, Springer. 89(1), pp. 87–90 (2017)
3. Yan, Y., Qian, Y., Sharif, H., Tipper, D. : A survey on smart grid communication infrastructures: Motivations, requirements and challenges. IEEE Commun. Surveys Tuts. 15(1), pp. 5–20 (2013)
4. Willig, A., Matheus, K., Wolisz, A.: Wireless technology in industrial networks. Proceedings of the IEEE. 93(6), pp. 1130–1151 (2005)
5. Luvisotto, M., Pang, Z., Dzung, D.: Ultra high performance wireless control for critical applications: Challenges and directions. J. IEEE Trans. Ind. Informat. 13(3), 1448–1459 (2017)
6. Pang, Z., Luvisotto, M., Dzung, D.: High Performance Wireless Communications for Critical Control Applications. J. IEEE Ind. Electron. Mag. (2017)
7. Rangan, S., Rappaport, T.S. and Erkip, E.: Millimeter-wave cellular wireless networks: Potentials and challenges. J. Proc. IEEE 102(3), 366–385 (2014)
8. Akdeniz, M.R., Liu, Y., Samimi, M.K., Sun, S., Rangan, S., Rappaport, T.S., Erkip, E.: Millimeter wave channel modeling and cellular capacity evaluation. J. IEEE J. Sel. Areas Commun. 32(6), 1164–1179 (2014)
9. Park, C., Rappaport, T.S.: Short-range wireless communications for next-generation networks: UWB, 60 GHz millimeter-wave WPAN, and ZigBee. J. IEEE Wireless Commun. 14(4) (2007)
10. Singh, S., Ziliotto, F., Madhow, U., Belding, E., Rodwell, M.: Blockage and directivity in 60 GHz wireless personal area networks: From cross-layer model to multihop MAC design. J. IEEE J. Sel. Areas Commun. 27(8), 1400–1413 (2009)
11. Shokri-Ghadikolaei, H., Fischione, C.: The transitional behavior of interference in millimeter wave networks and its impact on medium access control. J. IEEE Trans. Commun. 62(2), 723-740 (2016)
12. Thornburg, A., Bai, T., Heath, R. W.: Interference statistics in a random mmWave ad hoc network. In: IEEE International Conference on Acoustics, Speech and Signal Processing (ICASSP), pp. 2904–2908 (2015).
13. Singh, S., Kulkarni, M.N., Ghosh, A., Andrews, J.G.: Tractable model for rate in self-backhauled millimeter wave cellular networks. J. IEEE J. Sel. Areas Commun. 33(10), 2196–2211 (2015)
14. Bai, T., Heath, R. W.: Coverage and rate analysis for millimeter-wave cellular networks. J. IEEE Trans. Wireless Commun. 14(2), 1100–1114 (2015)
15. Di Renzo, M.: Stochastic geometry modeling and analysis of multi-tier millimeter wave cellular networks. J. IEEE Trans. Wireless Commun. 14(9), 5038–5057 (2015)
16. Niu, Y., Li, Y., Jin, D., Su, L., Wu, D.: Blockage robust and efficient scheduling for directional mmWave WPANs. J. IEEE Trans. Veh. Technol. 64(2), 728–742 (2015)
17. Shokri-Ghadikolaei, H., Fischione, C., Modiano, E.: On the accuracy of interference models in wireless communications. In: IEEE International Conference on Communications, pp. 1–6. Kuala Lumpur (2016)
18. El Ayach, O., Rajagopal, S., Abu-Surra, S., Pi, Z., Heath, R.W.: Spatially sparse precoding in millimeter wave MIMO systems. J. IEEE Trans. Wireless Commun., 13(3) 1499–1513 (2014)

19. El Ayach, O., Heath, R.W., Abu-Surra, S., Rajagopal, S. and Pi, Z.: The capacity optimality of beam steering in large millimeter wave MIMO systems. In: 13th IEEE International Workshop on Signal Processing Advances in Wireless Communications, pp. 100–104. Cesme (2012)